Staining Independent Nonrigid Iterative Registration Method, for Microscopic Samples

Róbert Paulik[1], Viktor Jónás[1], Miklós Vincze[2], Miklós Kozlovszky[2] and Béla Molnár[1]

[1] Image Analysis Department, 3DHISTECH Ltd., 1141 Budapest, Hungary; robert.paulik@3dhistech.com

[2] Department of BioTech Research Center, Óbuda University, 1034 Budapest, Hungary; kozlovszky.miklos@nik.uni-obuda.hu

Abstract: Using digital microscope scanners, gigapixel-scale images for tissue samples are scanned in a minute, which provides an opportunity for quantitative evaluation at the cellular or gene level. However, to make an accurate diagnosis for clinical or research cases, it is necessary to make serial sections and stain them using different reagents. Since digital scanning and processing are preceded by manual workflows, the orientations between the images are lost. In the absence of adjustment, we cannot compare them to each other, for colocalization or correlation analysis. A registration method is needed that organizes the samples in the same orientation. The proposed method is inspired by the traditional and deep-learning based registration methods (SURF, SIFT, ORB, SuperPoint, SuperGlue) and further developed to manage the tearing, creasing and other deformations between the samples. Based on the validation results, the basic methods give moderate results, however, by utilizing a grid-based approach and by choosing the appropriate number of recursive iterations and resolution, the methods can be improved. The proposed stain-independent, iterative, non-rigid registration method can manage not only tears, creases and deformations, but also correct structural changes between series sections.

Keywords: digital pathology; digital microscope; stain-independent; image registration; iterative; recursive; non-rigid; elastic; deep-learning; convolutional neural network

1 Introduction

The integration of digital imaging in medical diagnostics first began in radiology, and due to the benefits of the digital file, such as the ability to share, integrate, and archive, the same request has emerged in routine histopathology. The digital revolution began with the introduction of whole slide imaging (WSI) technology in pathology. Various scanner devices creating large files have been introduced, presenting tissue structures in an appropriate resolution with a high color fidelity [1] [2].

In digital pathology, sections stained with different reagents are used. To examine these sections together, it is necessary to register them with each other. Since the sectioning and floating up are manual and mechanical processes, the tissue sample can be deformed to a great extent by the time it is placed on the slide (Figure 1). Furthermore, if the physical distance between the sections was too large, they may not have the same structure visually. Similarly, different reagents may stain different tissue structures. Because of all this, we need a method that is flexible enough to register visually slightly different and deformed tissue sections.

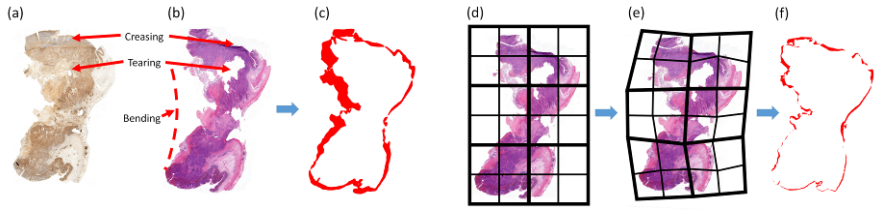

Figure 1

Illustration of deformations resulting from sample preparation and the required registration for correction: (a) source sample (MSH2 stained); (b) target sample (H&E stained); (c) difference of input samples; (d) Subdivided target sample; (e) registered target sample; (f) difference of registered samples

A fundamental problem with many computer vision tasks is finding visual correspondence between similar images. Stereo vision [3], object recognition [4], image stitching [5], visual odometry [6] are tasks which need a method for the registration problem. The feature extraction, description, matching and correspondence estimator methods were highly researched areas during the last three decades, many methods have been proposed that have sought a solution to these. Basically, the registration methods can be divided into three main categories: traditional feature-based approaches, deep-learning feature-based methods and homography learning.

Traditional feature-based algorithms, like Scale Invariant Feature Transform (SIFT) [7] and Speeded Up Robust Features (SURF) [8] methods are excellent feature detection, description, and matching algorithms, but even when an advanced matching process is applied, a considerable number of incorrect matches remains and needs to be eliminated. Random Sample Consensus (RANSAC) [9] is a widely used algorithm for removing false matches.

Nowadays, state-of-the-art methods in the field of image registration concern the use of deep learning. The Generic Feature Learning method [10] and SuperPoint approach [11] are using a training step of a convolutional neural network using only unlabeled public image datasets. SuperGlue network [12] is based on the SuperPoint “keypoint” detector and descriptor, which matches two pointset with a combination of Graph Neural Network and Optimal Matching layer. These methods can outperform the traditional methods; by resulting less outliers during the feature matching, the homography estimation can be more accurate.

Homography learning methods tries to solve the tasks of the previous methods in one step. They use a neural network to directly learn the transformation between an image pair. Deep Image Homography Estimation method [13] describes a regression homography network, a Visual Geometry Group (VGG) style model which is able to learn the homography by two images.

The previous registration methods are generally formulated as an optimization problem that satisfies constraints, such as coordinate displacements that are affine or volume preserving. Non-rigid and adaptive regularization methods [14] often outperform the traditional approaches in cases when the image pair contain non-linear and elastic deformations.

Some solutions found in the current literature try to perform the registration with a multi-modal approach [15] [16], with the help of which the samples with different colors can be registered to each other, but most of them use rigid registration and transformation.

We propose a novel approach, based on these traditional, deep-learning based and non-rigid solutions, enhanced with iterative and adaptive enhancements specialized for the registration of creased and torn tissue sections. The proposed method can also be useful in other disciplines, where it is needed to register samples that contain missing image parts to each other and their correct registration can only be solved by applying elastic transformation.

2 Materials and Methods

There are methods that perform registration on images, but it is exceedingly difficult to find a correspondence based on macrostructures in one step, which also gives satisfactory results in terms of microstructures. One reason for this is the tissue destruction [17] that occurs during sectioning, which can result in some regions of the sample being distorted, and another is due to the difference in staining [18], each reagent amplifies the tissue structures visually and differently.

Since there are many tissue samples that occur in real life that contain a large amount of tissue deficiency, according to our experience, homography learning approaches are not or only limitedly applicable, since these solutions can work well primarily when all the relevant details of the images are similar to each other. When there are too many torn and missing parts, they give an unsuccessful registration result. For this reason, the proposed approach relies more on the classical three-step approach, which is based on feature detection, correspondence and homography estimation, supplemented by a grid-based iterative method that ensures the flexible and non-rigid transformation (Figure 2).

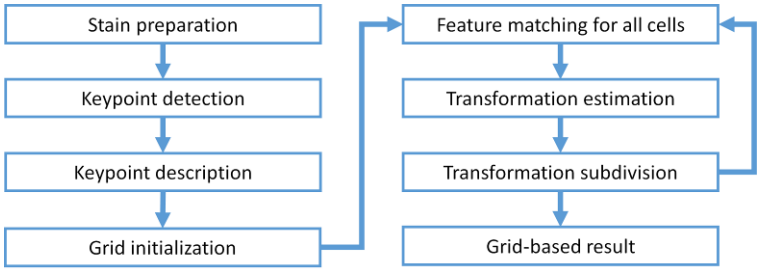

Figure 2
Algorithm overview of proposed method

2.1 Preparation Method

Since serial sections are often made to stain with different reagents, it is necessary to use a staining-independent preparation method to register them with each other. The proposed method uses an operation that tries to find visually similar-looking components between staining and then rely on them when registering. One of the most common such components is the nuclear-type structures [19] [20], which are present in both IHC [21] [22] (Immunohistochemistry) staining, and FISH [23] [24] (Fluorescence in situ hybridization) staining.

The proposed method uses a combination of two solutions for preparation of brightfield slides that have been extensively researched in other applications: staining unmixing [25-27] and staining normalization [28-31]. Staining unmixing or color deconvolution is a method used in brightfield microscopy to transform color images of multiple stained biological samples into images representing the stain concentrations. Staining normalization methods are designed to compensate the differences in intensity, saturation, and hue between samples, using a template image as a target image. These methods utilize color and spatial information to classify the image pixels into different stain components to reduce the effect of the variations of color and intensities which are caused by the sample preparation. Because the digitized image may contain significant amounts of camera noise, which may impair the efficiency of the recording, noise filtering, such as a median filter, may be required for some samples [32]. The chromatic and density distributions for the stain components in the hue-saturation-intensity color model are normalized to match with the distributions of a template image. In the case of a fluorescent sample, the proposed method uses the nuclei channel.

2.2 Keypoint Detectors and Descriptors

One of the basic ideas is to perform the registration in an iterative way in several steps: first detect an approximate transformation based on the larger

macrostructures, then further refine the registration considering the microstructures, trying to improve the result of the previous iteration in each iteration until it is possible.

The other basic idea is not to determine a single transformation value for the sample, but to assign different transformations to various parts of the sample. In this way, not only a rigid transformation with 6 or 8 degrees of freedom is performed, but an elastic deformation is used.

One of the most widely used traditional keypoint detector and descriptor algorithm is the scale-invariant feature transform (SIFT) [7] method. Although it is almost two decades old, has proven remarkably successful in several applications using visual features, including image stitching, object recognition, or stereo vision. However, the usage of it means a large computational requirement, which can be critical for systems which are real-time or has limited computational power.

This limitation was the cause of intense research in the direction of replacing it with a computationally more favorable alternative. One of the best alternatives are the Speeded Up Robust Features (SURF) [8], Features from Accelerated Segment Test (FAST) [33], Binary Robust Independent Elementary Features (BRIEF) [34] and Oriented FAST and Rotated BRIEF (ORB) [35] methods.

The ORB method has similar matching performance (Table 1) as the SIFT and SURF method but computationally it is more efficient. It utilizes the FAST method as keypoint detector and uses the BRIEF descriptor for feature description. These methods have superior performance and low computational cost. The ORB method adds a fast and accurate orientation component to the FAST method, optimizes the BRIEF feature computation, analyzes the variance and correlation of oriented BRIEF features, and to improve the performance of nearest-neighbor applications it has a learning method for de-correlating BRIEF features under rotational invariance.

Regarding the feature extraction and description, SuperPoint is one of the most state-of-the-art methods, which offers a fully convolutional model operates on full-sized images and computes pixel-level feature point positions together with their descriptions in one pass. In this study, we examine both the classical ORB method and the more modern SuperPoint approach as the basis of our method.

Table 1
Performance of keypoint detectors and descriptors

Method	Matching Performance	Computational Performance
SIFT	●●●○○	●●○○○
SURF	●●●○○	●●●○○
ORB	●●●●○	●●●●●
SuperPoint	●●●●●	●●●●○

2.3 Feature Matching and Transformation Estimation

After we detected features on the image pair and calculated descriptions for all of them, it is needed to match them. One of the simplest feature matching algorithms is the brute-force method [36], which takes descriptor of a feature on the first image and matches with all other features on the second image using distance calculation. It returns the closest pairs. When we matched the feature points on the image pair with each other, it is needed to estimate an optimal affine transformation (T) for them.

The widely used random sample consensus (RANSAC) [9] [37] method is a simple but effective iterative algorithm; it can estimate parameters of a mathematical model from a data set that contains outliers, when outliers are to be accorded no influence on the values of the estimates. Therefore, it also can be interpreted as an outlier detection method. In our case, we choose three keypoint matches at random and solve the T affine transformation as a system of equations. We count the number of matches which are inliers according to T transformation and distance limit. Repeat these steps for N rounds and return the T transformation which provided the highest inlier count.

2.4 Simple Grid-based Registration

The computed transformation matrix (T) can provide a good registration estimation for image pairs that include strictly only translational, rotational, and scaling differences. However, if the samples contain other types of deformations, the result may be inaccurate, or the result of RANSAC method may fail because choosing any of the three points will result too many outliers.

The proposed method utilizes grid-based registration, where we divide the image into smaller regions (patches), register these patches on their own, and then apply the separate transformations to the whole image like a grid (Algorithm 1).

Algorithm 1: Simple grid-based registration

Input: *matches, patches*

Output: *G* grid with affine transformation matrices

1. *G* = *patches* × *patches* empty grid
2. Forall *i* in 0..*patches*:
   2.1. Forall *j* in 0..*patches*:
      2.1.1. *roi* = Calculate ROI(*i, j, patches*)
      2.1.2. *matches'* = Collect matches in ROI(*roi*)
      2.1.3. *G*[*i, j*] = Estimate transformation(*matches'*)
3. Return *G*

2.5 Iterative Registration

One of the weaknesses of simple grid-based registration is that it can manage the non-linearity characteristics of the sample, but if we choose too large a grid size, there will be too little information available in a cell to perform the registration. In this case, we can only transform the cells by considering the local environment, so there may be many cells that you may not match properly or at all. If we choose a grid size that is too small, we will lose the ability to register nonlinear. In these cases, an iterative approach can help: the sample is first registered without a grid, in a rigid manner, considering all key points and the whole image (Figure 3).

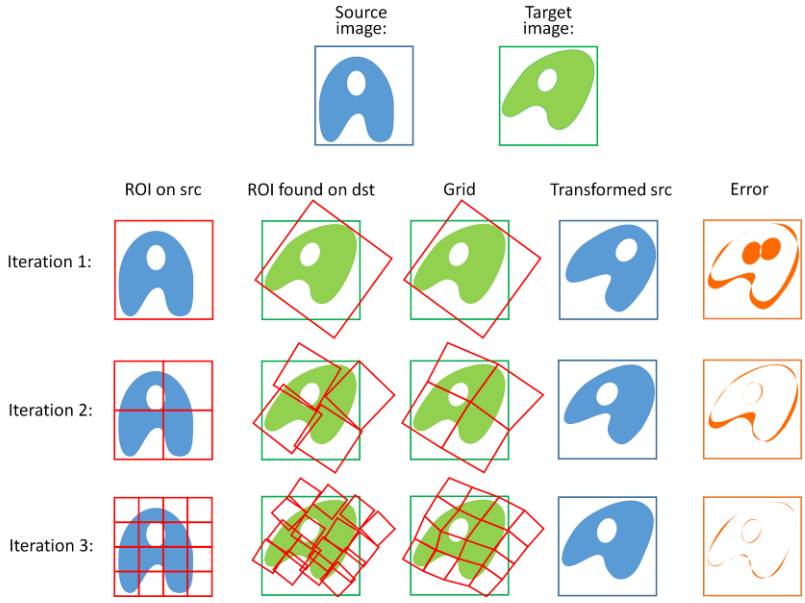

Figure 3
Illustration of iterative grid-based method

We assume that we can calculate globally the best possible rigid affine transformation. In the next iteration, the plane is divided into four equal parts, and the refined transformation matrices are calculated based only on the key points there but using the result of the previous iteration: only key pairs are considered whose transformed distance is less than a certain threshold. In the second iteration, we redistribute the previous four subdivided regions, so we will have a total of 16 regions, and we will also reduce the threshold used for the distance of the key points (Algorithm 2).

Algorithm 2: Recursive registration sub-method

Input: *matches*, *region, depth*

Output: *G* grid with affine transformation matrices

4. Filter the keypoints in the cell by their positions (*region*)
5. Filter the keypoints in the cell by their distances
6. T = Estimate transformations
7. If T is not valid:
   7.1. Return *Unit Matrix*
8. Decrease the distance limit
9. Apply *T* for *matches*
10. *G* = 2 × 2 empty subgrid
11. Forall *i, j*, *region'* in subdivide(*region*):
    11.1. *G*[*i, j*] = Recursive call with *depth'* and *depth+1*
12. Return *G*

Utilizing the recursive sub-method, we can calculate the elastic, non-rigid, grid-based registration (Algorithm 3).

Algorithm 3: Iterative grid-based registration method

Input: *img1*, *img2, depth*

Output: *G* grid with affine transformation matrices

1. *kp1* and *kp2* = Keypoint detection on *img1* and *img2*
2. *km* = Keypoint matching on *kp1* and *kp2*
3. G = Call the first iterative step

Return *G*

3 Validation

Routine anonymized slides were used from the archive of the 1st Department of Pathology and Experimental Cancer Research of the Semmelweis University, Budapest, Hungary. Digital slides in digital pathology are primarily identified by two key data: the inscription/barcode/QR code on the label area of the glass slide

and the name of the slide, often serving as a unique identifier. Using either of these, the patient can be traced back using the hospital information system. In case of research samples, both of these data are always removed right after (or before) scanning the samples. The samples providing the basis of this study were also de-identified and did not contain any details of the patient. The samples were used for a retrospective study without impacting patient care.

The study was conducted in accordance with the Declaration of Helsinki, approved by the Ethics Committee of the Institutional Review Board and Regional Ethics Committee of Semmelweis University (permit no. 14383-2/2017/EKU Semmelweis University, Budapest, Hungary).

Among the available samples, we collected cases in which there were at least 3 serial sections. It was important that these serial sections were not too far from each other in terms of distance, because that would make registration impossible (they cannot even be reconciled by humans in this case). Another aspect was that they should be stained with different reagents and that they should also have fluorescent sections.

A total of 268 slide pairs (53 slides from 12 cases) were selected for the validation and for each slide it was extracted only the scanned area in a size of 4000×4000 pixels (16 megapixels). This image size corresponds to a resolution of 4.185 µm/pixel on average. Images of this size clearly show larger and smaller tissue structures, but this resolution is too small to see cell compartments. The slides in the validation set were stained with 29 types of reagents.

Experts have placed five keypoints on each slide, in the middle of relevant regions or a well-defined part of slides. In the images belonging to the same cases, the same regions were marked. These regions were defined in such a way that both colleagues with biological and with bioengineering experience working in the field could mark them. Such areas were, for example, the center of a tumor area, the center of glands or border of a larger tissue region. The marking was performed at native resolution, and compared to the accuracy of the algorithm, the accuracy of the marking was an order of magnitude higher, so the consistency of the ground truth marking was not examined separately. Altogether it means 268×5 =1340 keypoint-pairs, they were used as a ground through during the validation.

Since the registration of slide pairs in the sample set is strongly influenced by whether they are pairs with the same staining and how they are prepared, we divided the image pairs into four categories (Figure 4):

a) Same staining and well prepared: Slide-pairs prepared with the same reagent, and they do not contain major creasing or tearing. It is usually easiest to register these samples together.

b) Same staining and creased/torn: The stainings are the same but the slide-pairs contain major tearing or creasing. With these samples, the need for an iterative approach can emerge.

c) Different staining and well prepared: The samples prepared correctly but the stainings are different.

d) Different staining and creased/torn: Samples with different stainings and contain major creases or tears. In general, these pairs are the most difficult to register with each other.

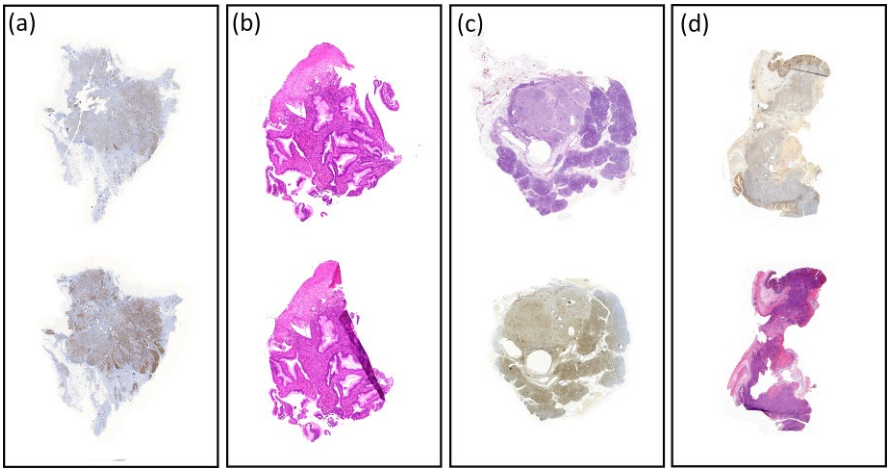

Figure 4

Illustration of the four sample categories: (a) same staining and well prepared; (b) same staining and creased/torn; (c) different staining and well prepared; (d) different staining and creased/torn

During validation, we examined the ideal resolution value and how the quality of the registration improves during the iterations. For scaling values, 1:1 resolution means the resolution of the input image (4.185 µm/pixel), 1:2 means half resolution (8.37 µm/pixel), until the 1:20 resolution (83.7 µm/pixel). Patch sizes 1, 2, 4, 8, 16, and 32 were examined for number of iterations. For optimal iteration number, 1, 2, 3, 4, and 5 iterations were examined, corresponding to 1×1, 2×2, 4×4, 8×8, 16×16, and 32×32 patches.

By validating the proposed method with each parameter, we compared the position of the keypoints marked by the experts with the positions transformed by the registration algorithm. From the distances, an error was calculated for each slide-pair using root mean squared error *(RMSE(c))* method, and then an average was calculated from them *(ARMSE)*.

Once the mean error *(ARMSE)* has been calculated for each number of scaling and iteration, we can determine their optimal values for our sample set. Both the mean error and standard deviation values are calculated back to µm/pixel.

Knowing the ideal parameters for the sample set, the proposed method is compared using the classic ORB keypoint detector and descriptor, the more modern SuperPoint algorithm and executing the SuperGlue approach.

4 Results

4.1 Optimal Number of Patches and Scale Factors

Table 2 shows the average root mean squared errors *(ARMSE)* of the registration using different patch numbers and scale factors. The lower value means the more precise registration. We can see that minimal value (137.12 µm) is reached using the parameters patches = 16 and scale = 1:6. Without iterative method (patches = 1) the error numbers are everywhere worse than with utilizing iterations. The average error *(ARMSE)* is the highest at 1:1 magnification without iterations (284.35 µm).

Table 2

Heatmap colorized table about the average root mean squared errors (ARMSE) using different scale factors and patch sizes. Lower and greener value means the more accurate registration. Values are in µm.

		Patches						
		1	2	4	8	16	32	Avg.:
1	1:1	284.35	244.05	237.55	233.11	233.34	235.34	**236.68**
2	1:2	233.75	195.87	187.04	184.26	181.38	169.59	**183.63**
3	1:3	215.32	176.27	165.27	163.02	162.99	154.67	**164.44**
4	1:4	196.24	159.99	150.11	148.05	147.49	142.09	**149.55**
6	1:6	179.83	149.22	139.19	138.70	137.12	147.50	**142.35**
8	1:8	179.47	152.84	141.25	141.07	139.81	147.89	**144.57**
10	1:10	177.67	151.22	144.31	143.05	141.41	149.37	**145.87**
12	1:12	180.46	157.09	145.39	144.66	146.65	144.89	**147.74**
14	1:14	179.80	152.63	143.38	140.37	140.19	156.43	**146.60**
20	1:20	182.92	161.73	152.43	153.24	154.12	153.68	**155.04**
	Avg.:	**200.98**	**170.09**	**160.59**	**158.95**	**158.45**	**160.14**	

(Scale)

As can be seen, the proposed method provides the lowest error value using patch-size 16×16 and scale factor 1:6. It corresponds to 5 iterations and 25.11 µm/pixel resolution.

A distance of 137.12 µm in terms of the error value means that there is an average difference of 137.12 µm between the ground truth manual alignment and the algorithmic result. This is a distance of approximately 10-15 nuclei. At the level of the cell compartment, it is therefore not possible to register the different sections using the method, but this is not the purpose of the registration; since there is a depth distance of 10-50 µm between the serial sections anyway, they will not have common nuclei anyway. In terms of macrostructures, however, it may be appropriate; their size is above this error value (e.g., glands), so they can be matched and examined together.

4.2 Optimal Number of Keypoints

Since the parameters scale = 1:6 and patches = 16 parameters proved to be the best, we examined the ideal keypoints number (Figure 5) with these parameters. The lowest number of keypoints examined was 200, while approaching a keypoint number of 10,000, the algorithm achieved the lowest error value: 137.12 µm. Using a higher keypoint count, the efficiency deteriorated again. There was no notable improvement in error value above 50,000 keypoints, suggesting that the sample contains an average of this number of usable key points.

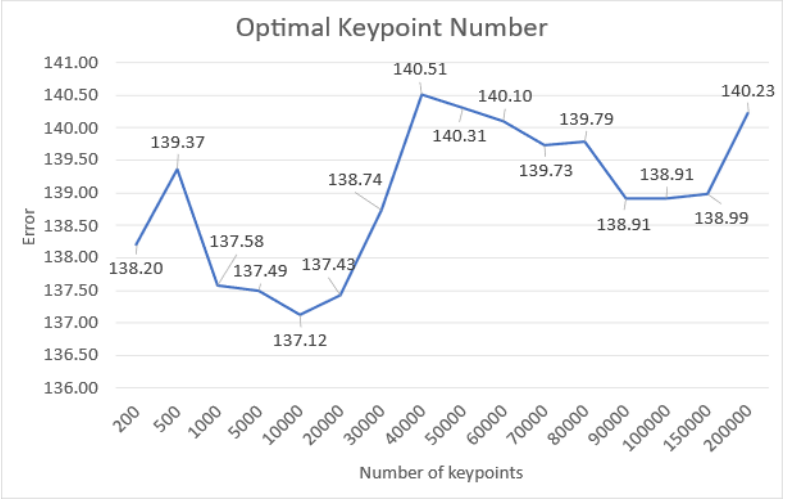

Figure 5
Average root mean squared error values *(ARMSE)* of using different number of keypoints. Values are in µm.

4.3 Average Error Values

Figure 6 shows the comparison of the average error values in each sample category applying the ORB based keypoint detection and description, the SuperGlue method, and the proposed method.

Analyzing the average error values, it can be concluded that the SuperGlue solution proves to be more effective in the case of well-prepared samples. However, in the case of samples that are not well prepared, i.e., contain creases or tears, the iterative nature of the proposed method can provide better results. The classic ORB key point detector always falls short of the results of the proposed method, it can only give similar results in the case of samples with same staining and well prepared.

Figure 6
Average root mean squared error values *(ARMSE)* applying different methods on sample categories. Values are in µm.

Looking at the results, it can be said that the proposed solution can bring better results mostly in the case of poorly prepared samples, under ideal conditions the SuperGlue solution may be sufficient.

4.4 Results Illustrations

To verify the robustness of image registration methods we compared the proposed method with the ORB keypoint detection using RANSAC matching algorithm, and with the SuperGlue registration method. Since the efficiency of the registration methods depends greatly on the quality of the sample preparation and staining, we separately analyzed the algorithms for identically stained and tear/crease-free samples and for differently stained and poorly prepared image-pairs. For demonstration purposes, the algorithm was also executed on high-resolution image pairs cut from whole slides.

Figure 7 shows the matching results in the case of five well-prepared and identically stained sections. It can be observed that usually the ORB+RANSAC based method provides 10-20 percent worse results than the proposed and SuperGlue approaches. Since these samples do not contain major tears or creases and visually look the same, the iterative nature of our method could not help, so the proposed method and SuperGlue approach provide similar results.

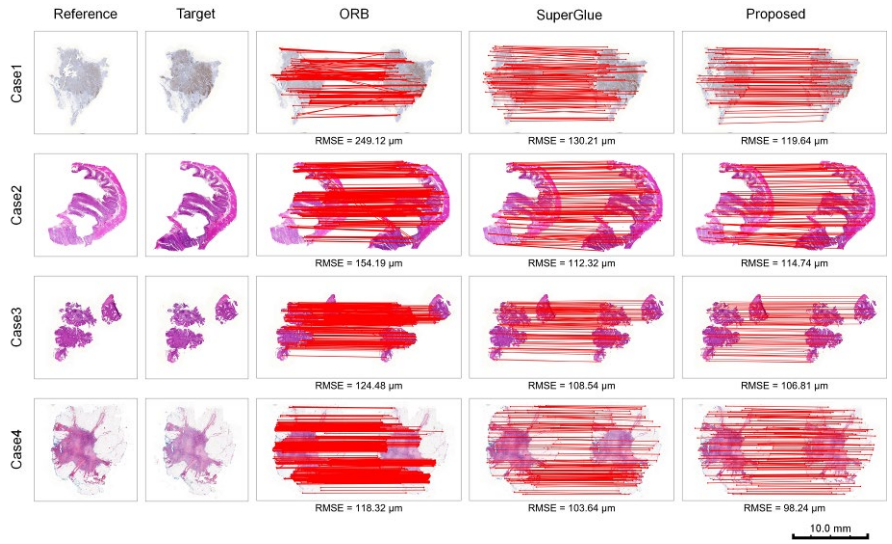

Figure 7
Matching results of five **well-prepared** and **identically stained** samples using the ORB+RANSAC, SuperGlue and proposed approaches

Figure 8 shows five examples, where the methods are executed on smaller parts of a whole slide image. The magnifications of these images are ten times larger than in Figure 7. These samples are also well-prepared and have the same staining. It can be observed that all three models provide similar results, this is due to the fact that the reference and target images are visually very similar.

In Figure 9, we can see the real differences between the analyzed models. In this picture we can see five samples, which are poorly prepared, containing tears and creases, and they are stained using different reagents. Since the image-pairs contain different tissue structures or have different colorizations, the classical ORB based method finds common feature points extremely hard and it matches them incorrectly. Compared to the proposed approach, the ORB method can achieve two-three times worse results on these samples than the proposed one. The iterative nature of the proposed approach can help these samples to a great extent, as in the first iteration it tries to find and match features on a low-resolution image that can be found on both images regardless of staining and tissue structure, and then this found similarity is further refined by further iterations. Using this approach, for image pairs that are difficult to register, the proposed approach mostly achieved better results than the SuperGlue solution.

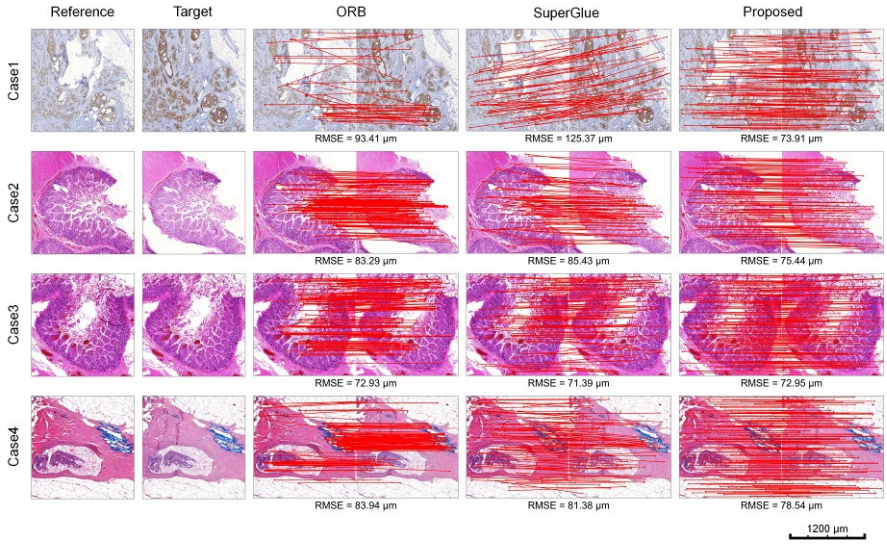

Figure 8
Matching results of five **well-prepared** and **identically stained high-resolution** samples using the ORB+RANSAC, SuperGlue and proposed approaches

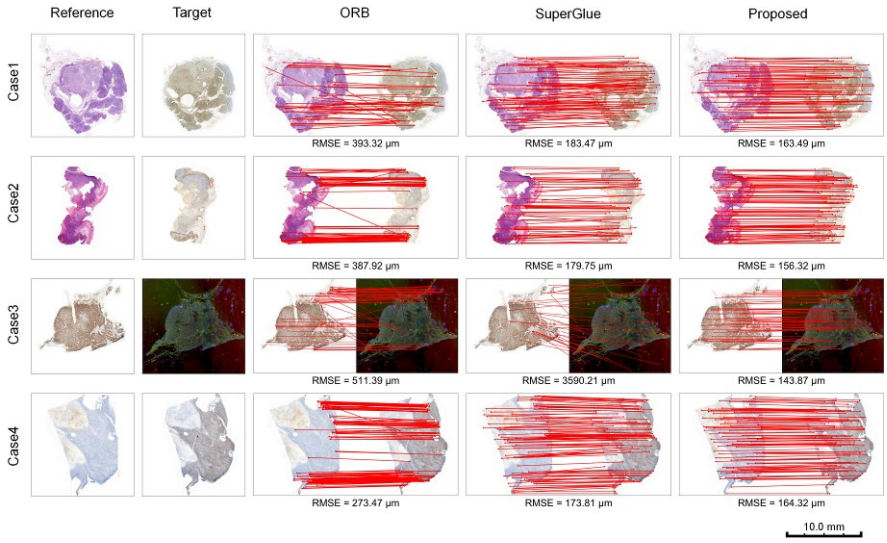

Figure 9
Matching results of five **differently stained** or **poorly prepared** samples using the ORB+RANSAC, SuperGlue and proposed approaches

From the illustration of results in Figure 10, it can be observed that the registration of high-resolution whole-slide parts are often unsuccessful, while the proposed method mostly can provide acceptable results. The reason for this is that ORB and SuperGlue methods do not have prior information about the approximate orientation of image parts and its key points, considering the whole-slide. In contrast to that the proposed method can know the rough position from the previous iterations, and it can consider the positions during the matching of keypoints.

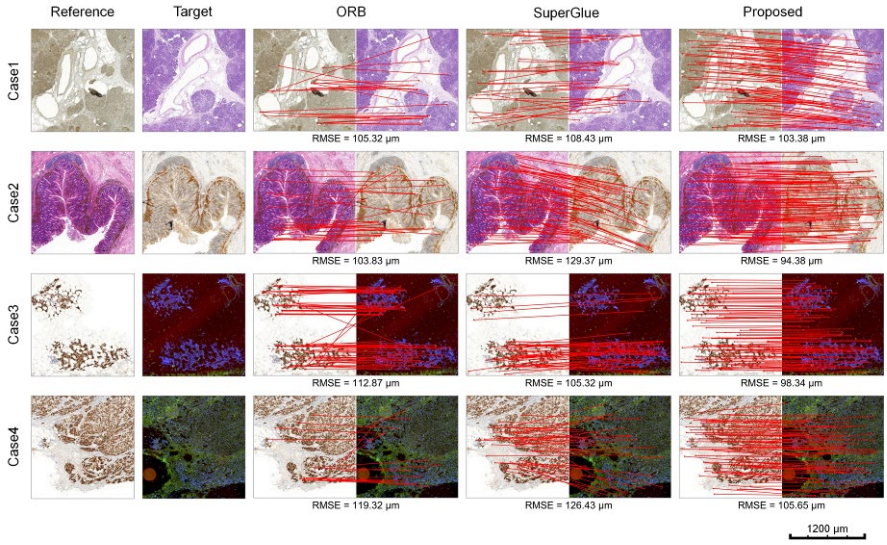

Figure 10

Matching results of five **differently stained** or **poorly prepared high-resolution** samples using the ORB+RANSAC, SuperGlue and proposed approaches

5 Discussion

The purpose of this study was to investigate how different registration methods perform in the task of aligning tissue samples onto each other in a whole slide imaging system and what parameters are used to achieve the best results. The proposed method was examined based on three main aspects and compared with competing solutions.

The first parameter examined was the value of the optimal patch number and scale factor, which was characterized by the mean squared error (ARMSE) metric, which gave the average accuracy of the registration expressed in microns. Based on our validation data set, the proposed solution achieved the best result using

16×16 patches (5 iterations) and a scale-factor value of 1:6, which resulted an error value of 137.12 μm.

The second examined parameter was the optimal number of keypoints, which was determined using the previously established patch and scale factor values. We analyzed key-points between 200 and 200,000, and the best performing key-point number was 10,000, where the proposed method achieved the best error value of 137.12 μm. It performed worse on fewer and more key-points than this.

The third evaluation method was a comparison with competitive solutions, where we examined the performance of the algorithm separately for the four types of samples, in comparison with the ORB-based and SuperGlue solutions. The results showed that under good conditions (with well-prepared samples) the SuperGlue solution gave the best results, however, for various types of stains and in the overall comparison, the proposed solution outperformed the others. The ORB-based solution fell short of the other two solutions in all categories. Overall, the recommended approach performs best in situations where an iterative approach is needed.

Registration is essential for making diagnosis or conducting research in serial sections. Because we used ground truth keypoints for validation, which experts laid down by marking the middle of the relevant regions, examining the results, we found that the appropriate scaling factor and grid-based iterative approach helped to perform the correct registration, thus helping the doctoral work.

However, it is important to mention that the parameters are strongly sample dependent. There are tissue samples that contain only a small amount of nonlinear distortion, either due to the thickness of the sample or due to better or more automated sample preparation. In this case, using a higher number of iterations is unnecessary. It is also important that some samples do not contain enough visual information to use the iterative method, and if you choose a patch number that is too high, there is a chance that they will be falsely registered, so the sample may be incorrectly deformed in those areas.

Analyzing the results of the validation set, several ideas have been put forward to improve the proposed methods. One such enhancement may be when the sample does not visually carry enough information or when completely different structural elements are painted between stains. Recognition of different tissue structures is a well-studied research field in the literature, with many approaches and methods already available from traditional pattern recognition algorithms [38] to sophisticated, deep learning based convolutional neural network methods [39-41]. By applying such methods on samples, we can detect features in the images that were not present locally at the pixel level and amplify similar areas of the different stained samples. By performing the proposed registration method on images prepared in this way, you can get better results.

Another improvement method is to try to use different magnifications between iterations. Initial iterations are often best recorded on low-resolution images, relying on macrostructures. However, this level of magnification no longer carries enough information in later iterations to calculate a more accurate transformation. To overcome this, we can try to use an increasingly high-resolution image as the basis between the iterations. A similar result can be obtained by using a key-point metric that carries information about a multi-resolution image, i.e., a multiscale feature.

Conclusions

The use of registration methods is critical for whole slide imaging (WSI), in the case of serial sections. In this study we collected a set of digital slides which required registration and after the implementation of registration method, we completed a validation study, to determine which model and which parameters provide the best results. According to the characteristics of the collected validation set, executing the methods, the following conclusions were drawn:

(1) For the registration of digital microscopic samples, the SuperPoint method is excellent for keypoint detection and description, supplemented with RANSAC-based keypoint pairing and affine transformation calculation. However, since not all parts of the sample are deformed in the same way during sample preparation, the transformation of the whole sample is not linear. In this case, the grid-based approach can be used to compute transformations for different regions of the sample separately.

(2) By choosing a high patch size, we can manage non-linearity, but there will be many patches that contain only microstructures, and without knowledge of the environment with macrostructures, we cannot accurately transform them into each other. The iterative approach can help the problem by initially performing the initial registration by choosing a low patch size and then further refining the regions by recursively redistributing them. The iterative approach performs non-rigid registration with more confidence and a lower error rate.

Acknowledgement

The authors would like to thank the expert colleagues who collected the samples representing the validation dataset and marked the ground-truth dataset: T.M. (pathologist, Semmelweis University) and G.K. (biologist, 3DHISTECH Ltd.).

This research was supported by the ÚNKP-22-3 New National Excellence Program of the Ministry for Culture and Innovation from the Source of the National Research, Development and Innovation Fund. The study received external funding from the national project 2019-1-3-1-KK-2019-00007.

References

[1] Krenacs, T.; Zsakovics, I.; Micsik, T.; Fonyad, L.; Varga, S. V.; Ficsor, L.; Kiszler, G.; Molnar, B. Digital microscopy – the upcoming revolution in histopathology teaching, diagnostics, research and quality assurance. *Microscopy: Science, Technology, Applications and Education Book Series,* **2010**, *Number 4*, 965-977

[2] Paulik, R.; Kozlovszky, M.; Molnár, B. Regression Based Iterative Illumination Compensation Method for Multi-Focal Whole Slide Imaging System. *Sensors,* **2021**, *21*, 7085, doi:10.3390/s21217085

[3] Song, H.; Xiao, H.; He, W.; Wen, F.; Yuan, K. A fast stereovision measurement algorithm based on SIFT keypoints for mobile robot. *2013 IEEE International Conference on Mechatronics and Automation,* **2013**, 1743-1748, doi:10.1109/ICMA.2013.6618179

[4] Lowe, D. G. Object recognition from local scale-invariant features. *Proceedings of the IEEE International Conference on Computer Vision,* **1999**, *2*, 1150-1157, doi:10.1109/ICCV.1999.790410

[5] Zhang, W.; Li, X.; Yu, J.; Kumar, M.; Mao, Y. Remote sensing image mosaic technology based on SURF algorithm in agriculture. *EURASIP Journal on Image and Video Processing* **2018**, *2018*, 85, doi:10.1186/s13640-018-0323-5

[6] Boulekchour, M.; Aouf, N.; Richardson, M. Robust L∞ convex optimisation for monocular visual odometry trajectory estimation. *Robotica,* **2014**, 1-20, doi:10.1017/S0263574714001829

[7] Lowe, D. G. Distinctive image features from scale-invariant keypoints. *International Journal of Computer Vision,* **2004**, 91-110, doi:10.1023/B:VISI.0000029664.99615.94

[8] Bay, H.; Tuytelaars, T.; Gool, L. Surf: Speeded up ro-bust features. *European Conference on Computer Vision,* **2006**, doi:10.1007/11744023_32

[9] Fischler, M. A.; Bolles, R. C. Random Sample Consensus: A Paradigm for Model Fitting with Applications to Image Analysis and Automated Cartography. *Comm. of the ACM,* **1981**, *24*, 381-395, doi:10.1145/358669.358692

[10] Dosovitskiy, A.; Fischer, P.; Springenberg, J.; Riedmiller, M.; Brox, T. Discriminative Unsupervised Feature Learning with Exemplar Convolutional Neural Networks. *IEEE Transactions on Pattern Analysis & Machine Intelligence,* **2016**, *38*, 1734-1747, doi:10.1109/TPAMI.2015.2496141

[11] DeTone, D.; Malisiewicz, T.; Rabinovich, A. SuperPoint: Self-Supervised Interest Point Detection and Description. *Proceedings of the IEEE*

Conference on Computer Vision and Pattern Recognition (CVPR) Workshops, **2018**, 224-236, doi:10.1109/CVPRW.2018.00060

[12] Sarlin, P.-E.; DeTone, D.; Malisiewicz, T.; Rabinovich, A. SuperGlue: Learning Feature Matching with Graph Neural Networks. *arXiv,* **2019**, doi:10.1109/CVPR42600.2020.00499

[13] DeTone, D.; Malisiewicz, T.; Rabinovich, A. Deep image homography estimation. *arXiv,* **2016**, doi:10.48550/arXiv.1606.03798

[14] Myronenko, A.; Song, X. Adaptive Regularization of Ill-Posed Problems: Application to Non-rigid Image Registration. *Comput. Res. Repos,* **2009**, *6*, doi:10.48550/arXiv.0906.3323

[15] Hoque, M. Z.; Keskinarkaus, A.; Nyberg, P.; Mattila, T.; Seppänen, T. Whole slide image registration via multi-stained feature matching. *Computers in Biology and Medicine,* **2022**, *144*, 105301, doi:10.1016/j.compbiomed.2022.105301

[16] Cooper, L.; Sertel, O.; Kong, J.; Lozanski, G.; Huang, K.; Gurcan, M. Feature-based registration of histopathology images with different stains: an application for computerized follicular lymphoma prognosis. *Comput Methods Programs Biomed,* **2009**, *96*, 182-192, doi:10.1016/j.cmpb.2009.04.012

[17] Taqi, S. A.; Sami, S. A.; Sami, L. B.; Zaki, S. A. A review of artifacts in histopathology. *J Oral Maxillofac Pathol,* **2018**, 22(2):279., doi:10.4103/jomfp.JOMFP_125_15

[18] Meyerholz, D. K.; Beck, A. P. Principles and approaches for reproducible scoring of tissue stains in research. *Laboratory Investigation,* **2018**, 98(7):844-855, doi:10.1038/s41374-018-0057-0

[19] Szenasi, S.; Vamossy, Z. Implementation of a Distributed Genetic Algorithm for Parameter Optimization in a Cell Nuclei Detection Project. *Acta Polytechnica Hungarica,* **2013**, *10*, 59-86, doi:10.12700/APH.10.04.2013.4.4

[20] Szenasi, S.; Vamossy, Z. Evolutionary Algorithm for Optimizing Parameters of GPGPU-based Image Segmentation. *Acta Polytechnica Hungarica,* **2013**, *10*, 7-28, doi:10.12700/APH.10.05.2013.5.2

[21] Gobbo, F.; Sarli, G.; Silva, M.; Galiazzo, G.; Chiocchetti, R.; Morini, M. A Double Histochemical/Immunohistochemical Staining for the Identification of Canine Mast Cells in Light Microscopy. *Vet. Sci,* **2021**, *8*, 229, doi:10.3390/vetsci8100229

[22] Smith, N. R.; Womack, C. A matrix approach to guide IHC-based tissue biomarker development in oncology drug discovery. *J Pathol,* **2014**, *Jan;232(2):190-8*, doi:10.1002/path.4262

[23] Frickmann, H.; Zautner, A. E.; Moter, A.; Kikhney, J.; Hagen, R. M.; Stender, H.; Poppert, S. Fluorescence in situ hybridization (FISH) in the microbiological diagnostic routine laboratory: A review. *Crit. Rev. Microbiol,* **2017**, *43*, 263-293, doi:10.3109/1040841X.2016.1169990

[24] Kuo, J.-T.; Chang, L.-L.; Yen, C.-Y.; Tsai, T.-H.; Chang, Y.-C.; Huang, Y.-T.; Chung, Y.-C. Development of Fluorescence In Situ Hybridization as a Rapid, Accurate Method for Detecting Coliforms in Water Samples. *Biosensors,* **2021**, *11*, 8, doi:10.3390/bios11010008

[25] Bianconi, F.; Kather, J. N.; Reyes-Aldasoro, C. C. Experimental Assessment of Color Deconvolution and Color Normalization for Automated Classification of Histology Images Stained with Hematoxylin and Eosin. *Cancers,* **2020**, *12*, 3337, doi:10.3390/cancers12113337

[26] Khan, A.; Rajpoot, N.; Treanor, D.; Magee, D. A nonlinear mapping approach to stain normalization in digital histopathology images using image-specific color deconvolution. *IEEE Trans. Biomed. Eng,* **2014**, *61*, 1729-1738, doi:10.1109/TBME.2014.2303294

[27] Ruifrok, A.; Johnston, D. Quantification of histochemical staining by color deconvolution. *Anal. Quant. Cytol. Histol,* **2001**, *23*, 291-299, pmid:11531144

[28] Bejnordi, E.; Babak; Litjens, G.; Timofeeva, N.; Otte-Höller, I.; Homeyer, A.; Karssemeijer, N.; Laak; Jeroen Stain Specific Standardization of Whole-Slide Histopathological Images. *IEEE transactions on medical imaging,* **2015**, *35*, doi:10.1109/TMI.2015.2476509

[29] Zheng, Y. Stain Standardization Capsule for Application-Driven Histopathological Image Normalization. *IEEE Journal of Biomedical and Health Informatics,* **2021**, *25*, 337-347, doi:10.1109/JBHI.2020.2983206

[30] Anghel, A.; Stanisavljevic, M.; Andani, S. A High-Performance System for Robust Stain Normalization of Whole-Slide Images in Histopathology. *Front Med Lausanne,* **2019**, *6*, doi:10.3389/fmed.2019.00193

[31] Balakrishnan, L.; Anand, S.; Jenitha, T. Stain Removal Through Color Normalization of Haematoxylin and Eosin Images: A Review. *Journal of Physics: Conference Series,* **2019**, *12108*, doi:10.1088/1742-6596/1362/1/012108

[32] Szántó, P.; Fehér, B. Hierarchical Histogram-based Median Filter for GPUs. *Acta Polytechnica Hungarica,* **2018**, *15*, 49-68, doi:10.12700/APH.15.1.2018.2.3

[33] Rosten, E.; Drummond, T. Machine learning for high-speed corner detection. *European Conference on Com-puter Vision,* **2006**, *1*, doi:10.1007/11744023_34

[34] Calonder, M.; Lepetit, V.; Strecha, C.; Fua, P. Brief: Binary robust independent elementary features. *In EuropeanConference on Computer Vision,* **2010**, doi:10.1007/978-3-642-15561-1_56

[35] Rublee, E.; Rabaud, V.; Konolige, K.; Bradski, G. ORB: an efficient alternative to SIFT or SURF. *Proceedings of the IEEE International Conference on Computer Vision,* **2011**, 2564-2571, doi:10.1109/ICCV.2011.6126544

[36] Jakubović, A.; Velagić, J. Image Feature Matching and Object Detection Using Brute-Force Matchers. *2018 International Symposium ELMAR,* **2018**, 83-86, doi:10.23919/ELMAR.2018.8534641

[37] Mac, T.; Lin, C.-Y.; Huan, N.; Luong, D.-N.; Hoang, P.; Hai, H. Hybrid SLAM-based Exploration of a Mobile Robot for 3D Scenario Reconstruction and Autonomous Navigation. *Acta Polytechnica Hungarica,* **2021**, *18*, 197-212, doi:10.12700/APH.18.6.2021.6.11

[38] Burges, C. J. A Tutorial on Support Vector Machines for Pattern Recognition. *Data Min. Knowl. Discov,* **1998**, *2*, 121-167, doi:10.1023/a:1009715923555

[39] Liu, X.; Song, L.; Liu, S.; Zhang, Y. A Review of Deep-Learning-Based Medical Image Segmentation Methods. *Sustainability* **2021**, *13*, 1224, doi:10.3390/su13031224

[40] Vu, Q. D.; Graham, S.; Kurc, T.; To, M. N. N.; Shaban, M.; Qaiser, T.; Koohbanani, N. A.; Khurram, S. A.; Kalpathy-Cramer, J.; Zhao, T. Methods for Segmentation and Classification of Digital Microscopy Tissue Images. *Front. Bioeng. Biotechnol,* **2019**, *7*, 53, doi:10.3389/fbioe.2019.00053

[41] Wetteland, R.; Engan, K.; Eftestøl, T.; Kvikstad, V.; Janssen, E. A. M. A Multiscale Approach for Whole-Slide Image Segmentation of five Tissue Classes in Urothelial Carcinoma Slides. *Technol. Cancer Res. Treat,* **2020**, 19, doi:10.1177/1533033820946787